Single Mode Fiber Optic Sagnac Interferometer with Wireless Data Collection

Doug Marett

Skyhunt, Toronto, ON Canada

Fiber optic Gyroscope, IFOG, FOG, Sagnac Interferometer, wireless data acquisition

Since the introduction of fiber optic gyroscope in the late 1970's [1], the need for accurate inertial navigational instruments has driven the evolution of the device into complex open or closed loop designs manufactured with expensive polarization maintaining fibers and fused fiber optic elements. Our goal herein is to describe a novel fiber optic Sagnac interferometer design made with readily available single mode (SM) components. The device utilizes a unique manual phase control method based on a single paddle fiber optic loop. This method allows the interferometer to be manually adjusted to the anti-phase condition prior to any measurements. Also described is the implementation of **a wireless data logger whose output can be displayed in Excel. Since the output voltage verses rotation rate is not linear, we further develop an equation predicting the expected voltage output verses angular velocity which matches a physical model of the superimposition of the counter-propagating waves at the photo-detector. We demonstrate a lack of Doppler shift in the rotating frame consistent with a classical explanation of the Sagnac effect.**

I. INTRODUCTION

A fiber-optic gyroscope (FOG) is a type of Sagnac interferometer which detects rotation by measuring the difference in the arrival time of two counter-propagating light beams circulating in a fiber-optic loop. The principle was first described in print by Georges Sagnac in 1913, using visible light travelling in a closed path, and subsequently the device is often referred to as a Sagnac interferometer, since light interference is the primary means of detecting the effect. [2] The principle works as follows: a light beam from a source (such as a laser) is split and the two beams are made to follow in opposite directions a trajectory that constitutes a ring. This ring encloses an area, but the axis of rotation doesn't have to be inside the area. The two light beams that exit the ring are made to interfere with each other, and the phase relation between the beams changes with the angular velocity which can be expressed visually or electronically. Most modern versions of the device apply frequency modulation to the beams prior to detection, preventing interpretation of the raw interference data. Our goal herein was to create a Sagnac device specifically intended for outputting unprocessed data, so that the characteristics of the returning beams can be studied directly. A block diagram of the fiber optic Sagnac interferometer is shown in Figure 1. Since another goal was to construct a low cost FOG, only optical parts available from commercial sources were used. The prevalence of fiber optic components in the 1.3 um band made this the ideal choice for our wavelength range.

Figure 1: Fiber optic Sagnac interferometer block diagram (all components co-rotate on a platform)

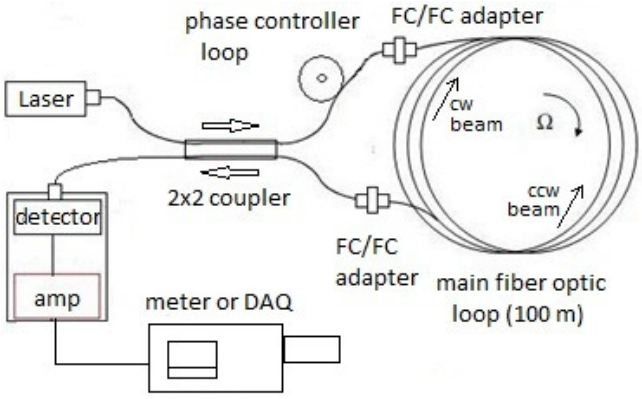

II. MATERIALS

The essential parts for this project were as follows:

FP-MQW 1.3 um laser with FC/PC connector

2 x 2 coupler (single mode) with FC/PC connectors

Phase controller loop and mount

100 m or 1000 m single mode fiber optic loop

PIN diode IR detector with amplifier

Output voltmeter or wireless DAQ

All of these components were sourced from local suppliers. The laser chosen was an FP-MQW type due to its low cost and availability pigtailed with an FC/PC connector. We also found that low cost DFB lasers were suitable. The power required was generally less than 1 mW output at 1.3 um, since too much power led to the saturation of the photodiode with subsequent loss of the interference signal. The use of corning smf-28 single mode fiber with 900um buffer throughout was the most suitable for reducing the bulk of the cable while maintaining adequate protection of the fiber.

III. METHODOLOGY AND TESTING

The optical components were mounted on an aluminum platform with predrilled mounting holes suitable for threading in 6-32 screws. Some ancillary components were 3D printed in house. This included mounting spools, the phase controller loop and meter mounts. The essential parts and hardware are shown in figure 2 below:

Figure 2: Parts for the Sagnac interferometer

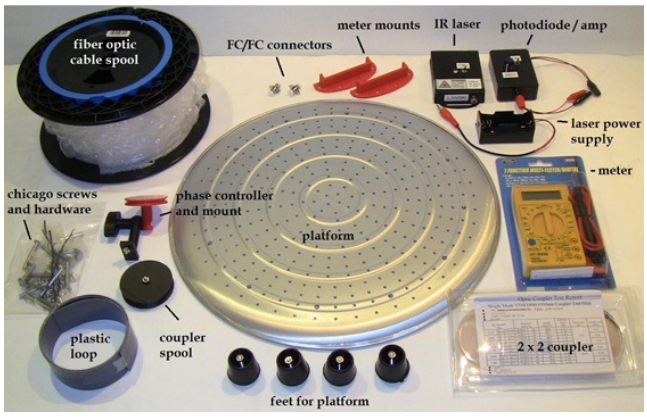

Construction consisted of first mounting a plastic loop onto the aluminum platform using Chicago screws, followed by wrapping the 100 m single mode cable around the loop. Since sensitivity increases with loop radius for a given rotation speed and loop length, it was decided to make the loop 16 cm in radius. Once the fiber loop was mounted, the rest of the optical components (laser, coupler, detector, and meter) were all screw-mounted inside the loop. For adjusting the phase balance between the two counter-propagating beams, a novel one paddle phase controller was designed and 3D printed. This consisted of a variable angle spool adjustable both vertically and horizontally (Fig. 3), with 2-3 loops of fiber wrapped around it from one side of the 2x2 coupler (just before the connection to the 100 m loop). This loop could be pivoted up and down in the vertical plane, inducing a variable stress birefringence in the fiber. This causes a phase relation shift between the counter-rotating beams, allowing the instrument to be tuned to the starting condition where the two beams are 180 degrees out of phase. The loop could then be locked in the desired orientation by tightening the handle.

Figure 3: Phase Controller Detail

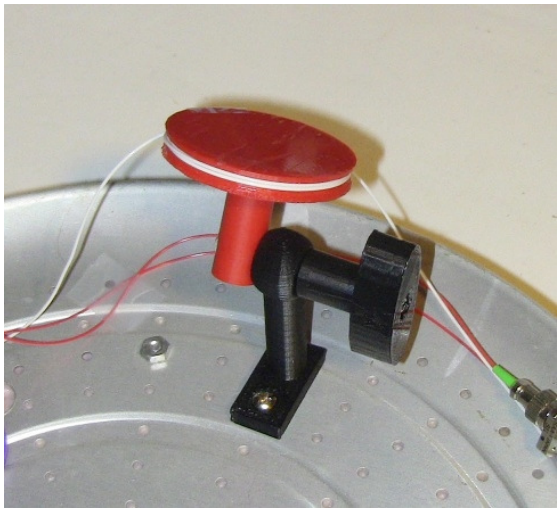

Although the interference voltage proportional to the phase difference can be read directly from the photodiode output when it is used in photovoltaic mode, there is usually a component of non-varying signal also present that prevents the output from ever reaching a zero mV output when the counter-propagating waves are out of phase. In order to solve this issue, the photodiode was followed with a common-mode rejection amplifier circuit that included a zero adjust to allow the output to be manually tuned to zero when the phase controller was adjusted such that the output was at its minimum. The assembled device is shown in figure 4:

Figure 4: Assembled Sagnac interferometer

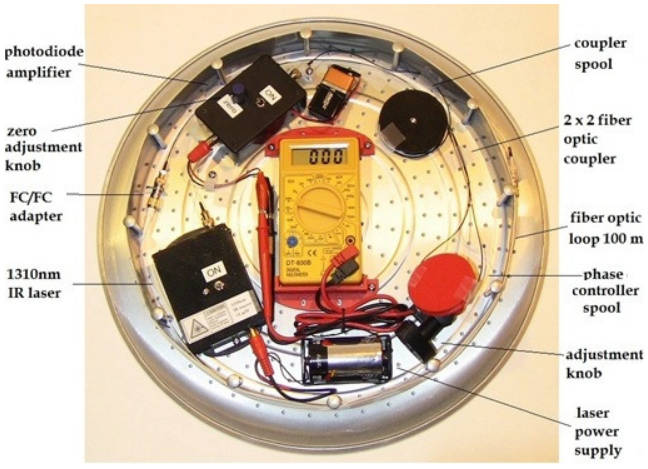

In this configuration, the amplified photodiode voltage was displayed directly on a voltmeter that was placed at the center of the device. This gives a reasonable qualitative display of the change in output voltage verses rotation speed that can be seen in real time. When the phase controller spool was adjusted to its minimum value it was typically 600-1000 mV on the meter prior to zeroing the amplifier. Once zeroed, rotating the device then causes the voltage output to rise from zero to a maximum of 1200 mV which then falls back towards zero as the speed increases further. This represents the progression of the counter-propagating waves from the out of phase condition to in phase, to out of phase again.

To make this effect more quantitatively visible, the voltmeter was replaced with a wireless data acquisition system (DAQ). Although such systems are available commercially, it was decided in this case to construct our own built around the 8 bit Microchip pic16F777 Flash microcontroller. This chip has built-in 10 bit A/D and is readily configured for outputting RS-232 data to a serial Bluetooth adapter. A software routine was written using a MPLAB ICD2 in circuit debugger which allowed for the device to send serial voltage data to a host computer wirelessly at 19200 Baud. A USconverters UCBT232B/EXA serial Bluetooth adapter was used with a Bluetooth USB dongle on the host computer, and raw data was received and stored using the program Putty. The raw data files were then converted to .csv format where they could be opened directly in Excel. The custom DAQ also transmitted time data for each data point collected, at a rate of 30 measurements per second, facilitating the production of detailed voltage verses rotational velocity curves in Excel.

IV. RESULTS

Data collected wirelessly is shown in figure 5. The fiber optic gyroscope was mounted on a turntable with a variable rotation speed adjustable between 0 and 87 RPM. The amplifier output from the PIN diode was adjusted to read zero volts when the turntable was stationary and the counter-propagating beams were in the out-of-phase condition. One channel of the DAQ was used to collect the amplified photodiode output, while a second channel was used to create RPM markers that generated a signal line (red) each time the interferometer completed one rotation. The turntable was set in rotation at its maximum speed and then allowed to slow down under low friction over a period of 30 seconds. As can be seen from the figure, the voltage output response (blue) was constant at 0.36V at the rotation rate of 87 RPM, and then followed a parabolic arc up to a maximum at 58 RPM before declining as the rotation rate fell to zero.

Figure 5: Interferometer output volts verses RPM collected using a wireless DAQ (100 m loop)

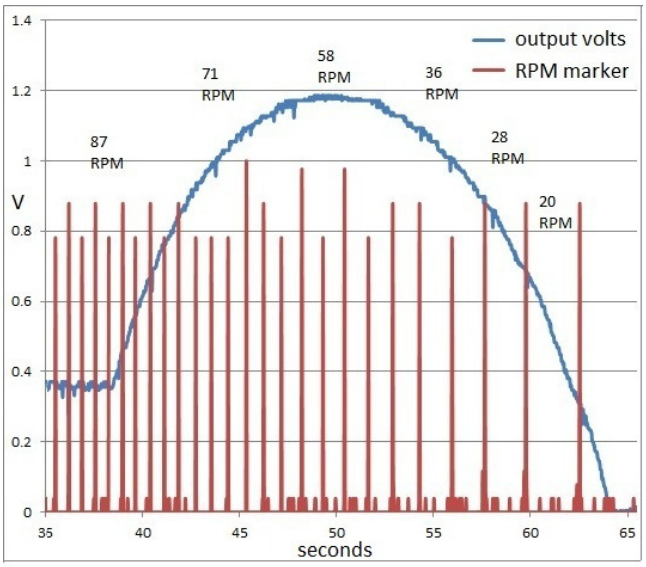

In a second series of tests, the 100 m loop was replaced with a 1000 m loop in order to increase the enclosed area by a factor of 10. This increased the sensitivity sufficiently so that it was possible to examine the voltage output profile over several fringe shifts in our chosen RPM range. This is shown in figure 6. The turntable rotation rate was increased from 0 to 107 RPM and the voltage output swept through 9.7 fringe shifts at the detector. The amplification was also increased in this test by about 3x in order to fully utilize the output voltage range of the wireless DAQ.

Figure 6: Interferometer output volts verses RPM collected using a wireless DAQ (1000 m loop)

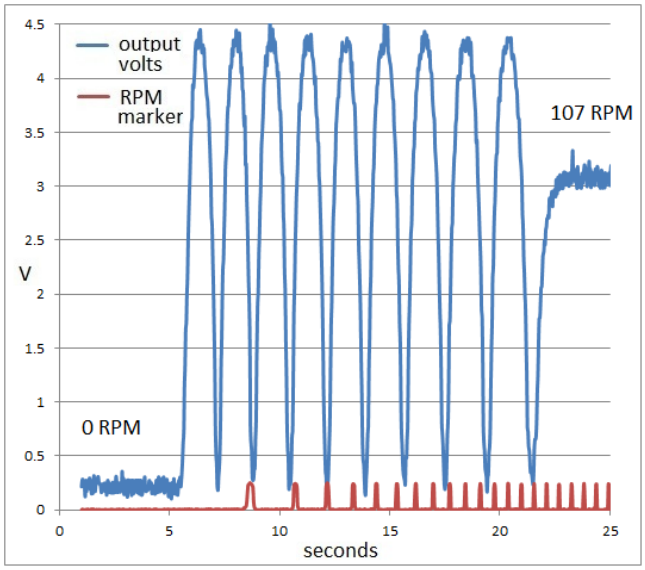

V. DISCUSSION

The voltage output observed from the device can be understood as the result of the superimposition of two counter-propagating waves at the photodetector, where a minimum output voltage corresponds to an out-of-phase condition, and the maximum voltage output the in-phase condition. As can be seen from figure 5, the in-phase condition corresponds to a rotational speed of around 58 RPM. The interferometer obeys the equations: [3]

$$\Delta t = \frac{4\omega A}{c^2} \qquad (1)$$

$$\Delta_{\text{fringe}} = \frac{4\omega A}{c\lambda} \qquad (2)$$

If the loop is 100 meters long and the radius (r) of the loop is 0.16 meters, the number of turns is about 100 (it is approximately 1 meter in circumference). For 360 degrees per second:

1) angular velocity ω would be $v/r = 6.25$
2) area $A = 0.08\ m^2 \times 100 = 8.04\ m^2$.
3) $C = 3 \times 10^8\ m/s$
4) $\lambda = 1.3 \times 10^{-6}\ m$

$$\Delta \text{ fringe} = 0.515$$

Since half of one fringe is a 180 deg. phase difference, then the voltage span from zero to maximum (out of phase to in phase) would occur at a rotation rate of:

$$360/(0.515x2) = 349.5 \text{ deg./s, or } 58.25 \text{ RPM}$$

as is observed in figure 5.

If the maximum voltage span is about 1200 mV, then this would give us a sensitivity of:

$$349.5/1200 = 0.29 \text{ deg./sec/mV}$$

Thereby a 1 mV change on the meter corresponds to a rotation rate difference of about 0.29 degrees/second. This gives a rough estimate of the sensitivity of the device to rotation. This voltage verses RPM response has been reproduced numerous times with a similar profile, and is easy to interpret.

As can be seen from figure 5, the voltage verses RPM response follows a parabolic curve which corresponds to the progressive superimposition of the counter-propagating waves from the out-of-phase condition (minimum voltage) to in-phase condition (maximum voltage) and back again as the RPM declines from 87 to zero. Due to this non-linear voltage response, the device sensitivity to rotation increases as the returning waves go out of phase. The progression across one full parabolic curve of voltage swing represents one full fringe shift of interference, so in the case of figure 5, the voltage swing from 0 RPM to 87 RPM represents about 80% of one interference fringe shift.

In the 1000 m loop length example of figure 6 the longer loop of cable made it possible to observe 9.7 interference fringe shifts at the detector. After considering the 10X larger area enclosed by the 1000 meter loop (or slightly more, due to the fiber bulk), this interference fringe shift corresponds very closely to 10x that of the interferometer with the 100 meter loop for the same RPM.

In order to properly explain the non-linear voltage output response, the light arriving at the photodetector was modelled as superimposed waves, where the voltage output is proportional to the sum of the constructive or destructive interference for a given phase difference between the waves at constant frequency. The following equation was derived to approximate the expected output voltage V:

$$V = \cos((\Delta\phi - \theta)/2) \times \text{range} \qquad (3)$$

Where:

range = the voltage difference between full destructive and full constructive interference as measured at the amplifier output.

$\Delta\phi$ = phase difference change between the counter-propagating waves in degrees due to rotation.

θ = the phase difference in the stationary state in degrees

The Sagnac fringe shift expression from (2) can then be incorporated into the equation expressed in (3) resulting in the equation below:

$$V = \cos\left(\frac{\frac{1440\,\omega A}{C\lambda} - \theta}{2}\right) \times \text{Range} \qquad (4)$$

Using the equation (4) it was then possible to create a theoretical response profile for the output voltage for a given fringe shift of the received waves at the photodetector. This theoretical profile matches quite closely the actual voltage output from the data logger, when compared to a sample fringe shift collected with the device operating with a 1000 m fiber loop. This is shown graphically in Figure 7.

It has been suggested by some authors that the Sagnac effect can be described as a form of Doppler Effect, or that the observer (detector) rotating with the fiber observes the equivalent of a frequency difference

Figure 7: Comparison of predicted output voltage profile against a sample fringe shift

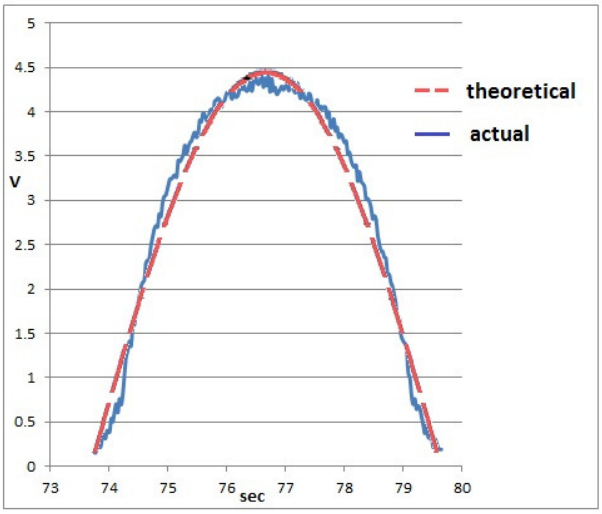

between the counter-propagating waves. [4] However, we have demonstrated experimentally herein that there is no frequency difference observed between the counter-propagating waves in the frame of the moving detector. Only a static phase difference is observed as is manifested in the unchanging phase voltage for a given RPM. If there was a frequency difference, this would appear as an AC voltage at the beat frequency between them. Dufour and Prunier in their comprehensive study of the Sagnac effect in 1942 demonstrated that this phase difference remains static (does not oscillate) even if the source or detector is stationary with respect to the rotating optical path. [5]

Since the counter-propagating waves share the same frequency in the rotating frame, and also typically the same optical path length (L), equation (1) can be expressed in a classical form (neglecting refractive index terms)[3,6]:

$$\Delta t = \frac{4\omega A}{c^2} = L/(c - \omega R) - L/(c + \omega R) \qquad (5)$$

The propagation times in the rotating frame for the two beams are not equal, since they equate to:

$$t_1 = L/(c - \omega R) \quad \text{co-rotating}$$
$$t_2 = L/(c + \omega R) \quad \text{counter-rotating} \qquad (6)$$

As a consequence, the speed of light measured by an observer in the rotating frame with his own clock will differ between the beams by the amount C+/- ωR. [3,6,7] This is also consistent with thermodynamics. Since light must obey the equation C = f * λ, the frequency f can't change between a co-moving source and receiver, since to do so would cause either a break in the wave-train or build-up of wave-crests at the detector, something which is thermodynamically impossible. However, in the Sagnac interferometer we see a wavelength difference Δλ between the counter-propagating waves as revealed in figures 5 and 6. In order to preserve C= f * λ, any change in λ where f remains constant demands that C also change to compensate, which is entirely consistent with equation (6). Engelhardt [7] has pointed out that applying the Lorentz transformation instead to the rotating frame results in a prediction of C = constant and thereby does not predict the Sagnac effect, since applying C = constant to equation (6) results in $t_1 - t_2 = L/c - L/c = 0$. The fact that the Sagnac interferometer demonstrates that the speed of light is not constant for the rotating observer is perhaps the device's most interesting feature.

VI. CONCLUSIONS

In this paper we have described a simple yet novel fiber optic Sagnac interferometer design. Utilizing our phase controller scheme, the device can be adjusted to the preferred stationary phase condition and generate electronic fringe shift data wirelessly as it rotates. The equation developed herein to express the electronic voltage verses rotation matches the experimentally derived curve. The lack of a demonstrable Doppler shift during device rotation is found to be consistent with the classical explanation of the Sagnac effect.

VII. ABBREVIATIONS

FOG, fiber-optic gyroscope; FP-MQW, Fabry-Perot multiple quantum well; FC/PC, ferrule connector polished contact; FC/FC, ferrule contact to ferrule contact adapter; IR, infrared; DAQ, data acquisition system; pic16F777, 8-bit microcontroller manufactured by Microchip Technology Inc.; 10-bit A/D, analog to digital converter with a resolution of 1024 units; RS-232, bi-directional serial communication protocol; MP-LAB ICD-2, a proprietary in-circuit program development tool manufactured by Microchip Technology Inc.; RPM, revolutions per minute.

VIII. REFERENCES

1. Bergh RA, Lefevre HC, Shaw HJ. Opt Lett. 1981; 6 10, 502-504.

2. Sagnac, G., Comptes Rendus 1913; 157: 708–710

3. Post, E. J., Rev. Modern Physics 1967; 39, 2, 475-493

4. Merlo, S., et.al. Handbook of Fiber Optic Sensing Technology. 2000; Wiley & Sons. Chapter 16.

5. Dufour, A., Prunier, F., J. de Physique. Radium 1942; 3 , 9, 153-162

6. Tartaglia, A., Ruggiero, M.L. 2014; arXiv.org: gr-qc/0401005

7. Engelhardt, W. 2014; arXiv.org:Ph-gen-ph:1404.4075